Acta Geologica Polonica, Vol. 69 (2019), No. 4, pp. 513–529
DOI: 10.24425/agp.2019.126441

Comparative geochemical assessment of jotunite rocks from the Suwałki Massif and the Sejny Intrusion (NE Poland)

ANNA GRABARCZYK[1] and JANINA WISZNIEWSKA[2]

[1] *Faculty of Geology, University of Warsaw, Żwirki i Wigury 93, PL-02-089 Warsaw, Poland.*
E-mail: anna.grabarczyk@student.uw.edu.pl
[2] *Polish Geological Institute – National Research Institute, Rakowiecka 4, PL-00-975 Warsaw, Poland.*
E-mail: jwis@pgi.gov.pl

ABSTRACT:

Grabarczyk, A. and Wiszniewska, J. 2019. Comparative geochemical assessment of jotunite rocks from the Suwałki Massif and the Sejny Intrusion (NE Poland). *Acta Geologica Polonica*, **69** (4), 513–629. Warszawa.

Jotunites (hypersthene monzodiorites/ferromonzodiorites) are rocks coeval with plutonic AMCG (anorthosite–mangerite–charnockite–rapakivi granite) suites, which are characteristic of the Proterozoic Eon. It has been experimentally shown that jotunite magma can be recognised as parental to anorthosites and related rocks: since then, research on these rocks has taken on a particular importance. Jotunites were recently described within the deeply buried c. 1.5 Ga Suwałki and Sejny anorthosite massifs in the crystalline basement of NE Poland. The major and trace element compositions of Polish jotunites show them to have a calc-alkalic to alkali-calcic and ferroan character, with a relatively wide range of SiO_2 content (40.56 wt. % up to 47.46 wt. %) and high concentrations of Fe (up to 22.63 wt. % Fe_2O_3), Ti (up to 4.34 wt. % TiO_2) and P (up to 1.46 wt. % P_2O_5). Slight differences in textural features, mineralogical compositions, and geochemistry of whole-rock jotunite samples from distinct massifs allow us to distinguish two kinds: a primitive one, present in the Sejny Intrusion, and a more evolved one, related to the Suwałki Massif.

Key words: Jotunites; Polish massif-type anorthosites; Parental magma; Primitive and evolved jotunites.

INTRODUCTION

Massif-type anorthosites and related rocks have been studied worldwide for over 100 years by numerous authors (see Ashwal 1993, 2010 for overview). Although many plausible origins have been postulated (Frost *et al.* 1989), none have given a convincing model of their formation. Several issues about the origin of these rocks have been debated, including: (1) What is the composition of the parental magma of anorthosites? (2) Where does the parental magma come from? (3) What is the mechanism that generated such huge volumes of feldspar cumulates? (4) What is the relationship between the felsic and basic members of the anorthosite–mangerite–charnockite –rapakivi granite (AMCG) suites? (5) Why are massif-type anorthosite intrusions restricted in age to the Proterozoic?

The AMCG magmatic association forms huge igneous complexes accompanied by minor amounts of intermediate rocks of hypersthene monzodioritic (jotunitic) composition. The discovery of jotunite rocks at the margin of andesine anorthosite bodies initiated a discussion about their meaning and possible models of their origin. It was argued that jotunites are: (1) transitional rocks in a comagmatic sequence from anorthosite to more felsic mangerite (Owens *et al.* 1993); (2) derived by the fractionation of mafic magmas unrelated to the anorthositic bodies (Emslie 1985); (3) derived from immiscible liquids conju-

gate to mangerites (Philpotts 1981); or (4) derived from residual liquids after anorthosite crystallization (Emslie 1978; Ashwal 1982; Emslie *et al.* 1994).

In the last case, a mantle-derived, Al-rich, basaltic parental liquid was postulated, which differentiates in a deep-seated magma chamber and crystallizes plagioclase (that accumulates at the roof of the intrusion) and mafic minerals (that sink down to the floor). The removal of mafic minerals leaves behind a residual melt of ferrodioritic composition. The plagioclases form a crystal mush that diapirically rises up to the level of final emplacement to build up anorthosite massifs. The ferrodioritic residual melt is entrained by the uprising plagioclase mush.

On the other hand, the lack of strong, visible, negative Eu anomalies in jotunites precludes a previous phase of plagioclase crystallization (Duchesne *et al.* 1974) and thus, a residual origin. Consequently, jotunites were also considered as (5) parental to andesine-type anorthosites (Duchesne and Demaiffe 1978). This conclusion was later confirmed experimentally (Vander Auwera and Longhi 1994; Longhi *et al.* 1999).

Anorthosites reveal evidence of polybaric emplacement, as indicated by the occurrence of high alumina orthopyroxene megacrysts (Emslie 1975; Fram and Longhi 1992), shown experimentally to have equilibrated at a lower crustal pressure of 11–13 kbar and then brought to their final level of crystallization, which took place at depths corresponding to 3–5 kbar pressure (Longhi *et al.* 1999). Diapiric emplacement is additionally confirmed by the appearance of kinked plagioclase crystals, caused by the ascent of the crystal mush into a shallower part of the crust (Wiszniewska *et al.* 2002). Moreover, it is now widely accepted that the occurrence of anorthosite massifs is connected with weakness zones in the lithosphere (Duchesne *et al.* 1999), which were migration paths and led to the emplacement of the crystal mush into the upper part of the crust. This idea supported the model of underthrusting of a crustal tongue of dry, mafic rocks and their partial melting at 10–13 kbar to give jotunitic parent magmas (Duchesne *et al.* 1999).

When jotunites were found in the Suwałki and Sejny massifs in NE Poland (Wiszniewska *et al.* 2002), it became very tempting to consider jotunitic magma as parental for the Suwałki and Sejny anorthosites, as well.

GEOLOGICAL FRAMEWORK

The Suwałki Anorthosite Massif (SAM) and the Sejny gabbro–norite intrusion are located in NE Poland (Text-fig. 1) and belong to the south-western zone of the East European Craton (EEC; e.g., Bagiński *et al.* 2007). This area of the EEC is covered by non-metamorphosed Phanerozoic platform sediments of variable thickness, from 500 m in NE Poland up to 6–8 km along the Trans-European Suture Zone at the SW margin of the EEC (Ryka 1993). The recognition of deep basement structures is possible only through interpretation of geophysical data and from direct petrological and geochemical studies of drill cores (Bagiński *et al.* 2007) from about 250 deep boreholes, distributed unevenly throughout the area (Wiszniewska and Krzemińska 2005).

Both the SAM and the Sejny Intrusion, together with the Kętrzyn Anorthosite Massif located to the west, are connected with different kinds of rapakivi-like granitoids of A-type affinity (Bagiński *et al.* 2001; Gawęda *et al.* 2009; Duchesne *et al.* 2010), and belong to the so-called Mazury Complex (Text-fig. 1). This structure forms a 200 km long belt associated with an E–W-trending older, later rejuvenated, deep crustal lineament (Kubicki and Ryka 1982; Bagiński *et al.* 2001; Cymerman 2014), active for approximately 15 million years (Morgan *et al.* 2000; Duchesne *et al.* 2010). The Mesoproterozoic, c. 1.5 Ga (Claesson *et al.* 2001) Mazury Complex intruded Palaeoproterozoic granulite-facies metamorphic complexes (Text-fig. 1) of the West Lithuanian Domain (Duchesne *et al.* 2010). The Kętrzyn Massif and the SAM show a diapiric character in cross-section (Juskowiak 1998). Later, post-magmatic deep erosion of the crystalline basement (Ryka 1998) exposed the concentric shape of the intrusions (Text-fig. 1), where an anorthositic centre, with some Fe-Ti deposits, is surrounded by norite, gabbro and diorite, the latter additionally crosscut by thin dyke-like jotunites. This petrology points to the presence of an AMCG suite characteristic of Proterozoic domains (Taylor *et al.* 1984; Ashwal 2010). Recent Re-Os isochron ages of 1559 ± 37 Ma have been obtained on oxide and sulphide minerals from the ore deposits in the SAM (Stein *et al.* 1998; Morgan *et al.* 2000; Wiszniewska *et al.* 2002) and extended onto the age of the anorthosites. All these features make the SAM and the Sejny Intrusion perfect objects for detailed studies on the origin and evolution of anorthosite massifs.

The samples used in this paper come from five boreholes located within the SAM and the Sejny Intrusion: Bilwinowo IG-1 (southern part of SAM; B1), Jezioro Szlinokiemskie IG-1 (eastern part of SAM; JS1) and Udryń 11 (centre of SAM; U11), and the Sejny IG-1 (S1) and Sejny IG-2 (S2) boreholes, respectively. Additionally, two major almost N–S-

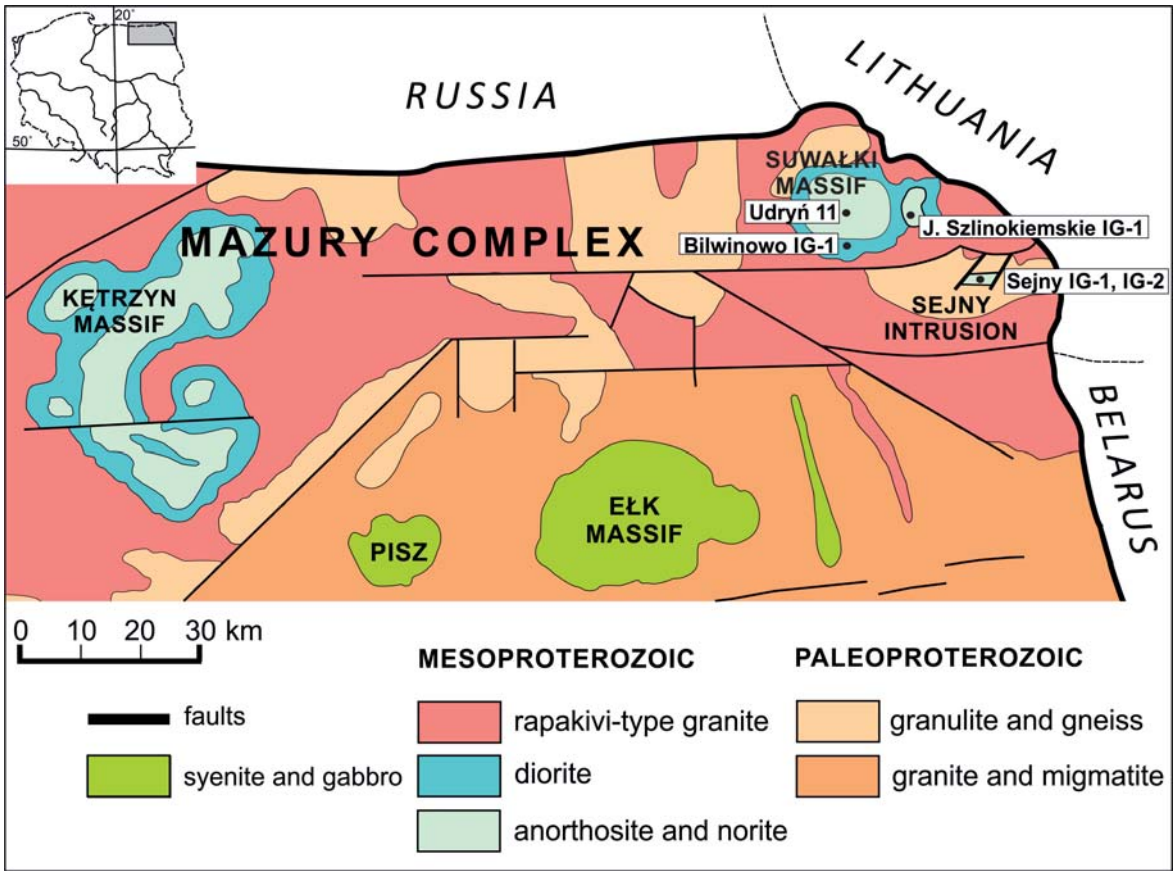

Text-fig. 1. Schematic geological map of the Mazury Complex, essentially composed of rapakivi and rapakivi-like granites, three anorthosite massifs (Suwałki, Sejny and Kętrzyn) and related rocks. The boreholes from which the samples studied here have been collected (Bilwinowo IG-1, Udryń 11, Jezioro Szlinokiemskie IG-1, Sejny IG-1 and Sejny IG-2) are indicated (after Wiszniewska *et al.* 2002; modified)

trending discontinuities subdivide the SAM into three blocks (Cieśla *et al.* 1998), placing the Udryń 11 and Bilwinowo IG-1 boreholes in the western block and the Jezioro Szlinokiemskie IG-1 borehole in the eastern block (Text-fig. 1).

METHODS

Quantitative chemical data were acquired using a CAMECA SxFive FE electron microprobe at the Inter-Institute Analytical Complex for Minerals and Synthetic Substances, University of Warsaw. The following standards, analytical lines, and crystals were used: albite – Na (Kα, LTAP), orthoclase – Al (Kα, TAP), albite – Si (Kα, TAP) for feldspars, diopside – Si (Kα, TAP) for pyroxene, orthoclase – K (Kα, LPET), Fe_2O_3 – Fe (Kα, LLIF), diopside – Mg (Kα, LTAP), rhodonite – Mn (Kα, LLIF), diopside – Ca (Kα, LPET), TiO_2 – Ti (Kα, LPET), Cr_2O_3 – Cr (Kα, LLIF), CoO – Co (Kα, LLIF), NiO – Ni (Kα, LLIF), crocoite – Pb (Mα, LPET), $SrBaNb_4O_{12}$ – Ba (Lα, LPET), $SrBaNb_4O_{12}$ – Sr (Lα, TAP) and Rb(Ge-Al-Ca) glass – Rb (Lα, LTAP). Analyses were conducted using an accelerating voltage of 15 kV and beam current of 10 nA (for feldspars) and 15nA (for pyroxenes). ZAF corrections were applied. The standard deviation was set at 1Σ. Fe^{2+}/Fe^{3+} ratio estimates were made on the basis of Droop's (1987) method. The results are presented in Tables 1–3.

Whole-rock samples from the Bilwinowo IG-1, Udryń 11, Jezioro Szlinokiemskie IG-1, Sejny IG-1 and Sejny IG-2 boreholes were analysed for major and some trace elements in ACME Analytical Laboratories (now Bureau Veritas Minerals) and in the laboratory of the Polish Geological Institute – National Research Institute (PGI-NRI). Major elements were analysed using ICP-ES and trace elements were analysed using ICP-MS. The chemical compositions are presented in Tables 4–6.

wt.%	1	2	3	4	5	6	7	8	9	10	11	12	13	14	15	16	17	18
SiO_2	56.78	58.41	58.27	57.25	57.08	57.80	50.98	57.58	57.11	58.06	58.34	58.27	57.99	58.15	58.08	57.77	57.97	56.93
Al_2O_3	26.73	25.94	26.13	26.63	26.81	26.25	30.43	26.42	26.75	26.00	26.01	25.77	26.36	26.59	26.26	26.65	26.37	27.08
FeO	0.15	0.14	0.11	0.13	0.15	0.14	0.19	0.12	0.20	0.14	0.14	0.11	0.13	0.16	0.13	0.19	0.14	0.19
CaO	9.60	8.69	8.84	9.42	9.55	9.02	14.01	9.40	9.67	8.72	8.73	8.82	9.15	8.98	9.03	9.33	9.03	9.76
SrO	0.14	0.16	0.12	0.15	d.l.	0.15	0.13	0.13	0.16	0.17	0.16	0.15	0.19	0.14	0.14	0.16	0.13	0.16
Na_2O	5.30	5.77	5.51	5.72	5.60	5.84	3.28	5.73	5.62	5.75	5.79	5.56	5.57	5.43	5.53	5.50	5.56	5.17
K_2O	0.38	0.36	0.36	0.37	0.16	0.20	0.06	0.35	0.33	0.37	0.40	0.40	0.40	0.34	0.37	0.28	0.34	0.39
Rb_2O	0.14	0.16	0.17	0.11	0.15	0.11	0.12	0.11	0.11	0.15	0.17	0.16	0.12	0.14	0.12	0.12	0.13	0.13
Total	99.22	99.63	99.51	99.77	99.48	99.50	99.19	99.84	99.94	99.34	99.73	99.24	99.90	99.93	99.66	100.00	99.65	99.80
apfu																		
Si^{4+}	2.570	2.624	2.619	2.578	2.573	2.602	2.341	2.589	2.569	2.617	2.620	2.627	2.602	2.604	2.609	2.590	2.604	2.562
Al^{3+}	1.426	1.373	1.384	1.413	1.424	1.393	1.646	1.400	1.418	1.381	1.376	1.369	1.394	1.403	1.390	1.408	1.396	1.436
Fe^{2+}	0.006	0.005	0.004	0.005	0.006	0.005	0.007	0.005	0.008	0.005	0.005	0.004	0.005	0.006	0.005	0.007	0.005	0.007
Ca^{2+}	0.466	0.418	0.426	0.455	0.461	0.435	0.689	0.453	0.466	0.421	0.420	0.426	0.440	0.431	0.434	0.448	0.435	0.471
Sr^{2+}	0.004	0.004	0.003	0.004	0.000	0.004	0.003	0.003	0.004	0.004	0.004	0.004	0.005	0.004	0.004	0.004	0.003	0.004
Na^{+}	0.465	0.503	0.480	0.499	0.489	0.510	0.292	0.499	0.490	0.502	0.504	0.486	0.485	0.471	0.482	0.478	0.484	0.451
K^{+}	0.022	0.020	0.021	0.021	0.009	0.012	0.003	0.020	0.019	0.021	0.023	0.023	0.023	0.019	0.021	0.016	0.020	0.022
Rb^{+}	0.004	0.005	0.005	0.003	0.004	0.003	0.003	0.003	0.003	0.004	0.005	0.005	0.003	0.004	0.004	0.004	0.004	0.004
Total	4.962	4.953	4.942	4.978	4.966	4.964	4.986	4.972	4.978	4.956	4.958	4.945	4.956	4.942	4.949	4.955	4.951	4.958
An%	48.91	44.43	45.92	46.62	48.09	45.49	70.02	46.55	47.80	44.57	44.33	45.54	46.45	46.74	46.34	47.58	46.33	49.84
Ab%	48.80	53.41	51.84	51.19	50.97	53.29	29.65	51.37	50.25	53.20	53.22	51.99	51.17	51.15	51.39	50.74	51.59	47.80
Or%	2.29	2.16	2.23	2.19	0.94	1.23	0.33	2.08	1.95	2.23	2.44	2.47	2.39	2.10	2.27	1.68	2.08	2.36

Table 1. Representative electron microprobe analyses (EMPA) of plagioclase from the Bilwinowo IG-1 borehole (SAM); d.l. – below detection limit

wt.%	1	2	3	4	5	6	7	8	9	10	11	12	13	14	15
SiO_2	65.52	65.39	66.36	66.07	66.09	65.49	66.46	66.14	66.63	66.91	66.07	65.98	65.87	64.49	64.58
Al_2O_3	18.05	18.09	18.11	17.99	18.08	17.93	18.24	18.09	18.31	18.44	18.24	18.21	18.19	18.33	18.28
CaO	d.l.	d.l.	d.l.	d.l.	d.l.	d.l.	d.l.	d.l.	d.l.	d.l.	d.l.	d.l.	d.l.	d.l.	d.l.
SrO	0.26	0.25	0.24	0.25	0.23	0.23	0.28	0.24	0.27	0.26	0.30	0.25	0.28	0.27	0.26
BaO	0.94	0.88	0.84	0.85	0.92	0.93	0.96	0.90	1.14	1.12	1.04	0.95	1.05	2.19	2.04
Na_2O	0.29	0.25	0.29	0.29	0.23	0.23	0.29	0.22	0.58	0.51	0.47	0.40	0.42	0.89	0.93
K_2O	15.50	15.31	14.52	14.55	14.46	15.37	14.46	14.49	14.06	13.93	14.09	14.17	14.11	14.05	14.16
Rb_2O	0.16	0.19	0.19	0.19	0.19	0.17	0.18	0.20	0.13	0.15	0.16	0.17	0.13	0.13	0.16
Total	100.72	100.35	100.55	100.19	100.19	100.37	100.85	100.28	101.11	101.31	100.36	100.13	100.05	100.34	100.42
apfu															
Si^{4+}	3.018	3.018	3.037	3.037	3.036	3.024	3.034	3.036	3.032	3.034	3.030	3.031	3.030	2.995	2.997
Al^{3+}	0.980	0.984	0.977	0.975	0.979	0.976	0.981	0.979	0.982	0.985	0.986	0.986	0.986	1.003	0.999
Ca^{2+}	0.000	0.000	0.000	0.000	0.000	0.000	0.000	0.000	0.000	0.000	0.000	0.000	0.000	0.000	0.000
Sr^{2+}	0.007	0.007	0.006	0.007	0.006	0.006	0.007	0.006	0.007	0.007	0.008	0.007	0.007	0.007	0.007
Ba^{2+}	0.017	0.016	0.015	0.015	0.016	0.017	0.017	0.016	0.020	0.020	0.019	0.017	0.019	0.040	0.029
Na^{+}	0.026	0.022	0.026	0.026	0.020	0.021	0.025	0.020	0.051	0.045	0.042	0.036	0.038	0.080	0.084
K^{+}	0.911	0.901	0.848	0.853	0.848	0.905	0.842	0.849	0.816	0.806	0.824	0.831	0.828	0.833	0.838
Rb^{+}	0.005	0.006	0.006	0.005	0.006	0.005	0.005	0.006	0.004	0.004	0.005	0.005	0.004	0.004	0.005
Total	4.963	4.954	4.914	4.918	4.911	4.954	4.912	4.912	4.912	4.901	4.913	4.912	4.912	4.962	4.967
An%	0.00	0.00	0.00	0.00	0.00	0.00	0.00	0.00	0.00	0.00	0.00	0.00	0.00	0.00	0.00
Ab%	2.76	2.38	2.94	2.96	2.34	2.24	2.92	2.27	5.89	5.30	4.85	4.15	4.36	8.81	9.08
Or%	97.24	97.62	97.06	97.04	97.66	97.76	97.08	97.73	94.11	94.70	95.15	95.85	95.64	91.19	90.92

Table 2. Representative electron microprobe analyses (EMPA) of K-feldspar (antipertite) from the Bilwinowo IG-1 borehole (SAM); d.l. – below detection limit

wt.%	1	2	3	4	5	6	7	8	9	10	11	12	13	14	15	16	17	18
SiO_2	50.77	50.53	50.45	50.39	50.78	50.54	51.23	50.60	50.86	51.24	51.01	50.22	50.40	51.09	50.35	50.80	50.90	50.82
TiO_2	0.12	0.10	0.11	0.09	0.08	0.08	0.07	0.08	0.08	0.07	0.09	0.31	0.26	0.20	0.25	0.30	0.25	0.20
Al_2O_3	0.94	0.87	0.82	0.99	0.83	0.85	0.75	0.85	0.81	0.82	0.86	1.81	1.71	1.51	1.70	1.77	1.68	1.56
FeO	25.88	25.97	26.16	25.91	26.23	26.39	25.36	26.32	25.83	25.62	26.16	10.25	9.52	10.19	9.67	10.55	12.14	9.71
MnO	1.13	1.12	1.14	1.12	1.06	1.13	1.25	1.14	1.11	1.27	1.23	0.50	0.41	0.49	0.43	0.47	0.45	0.41
MgO	19.42	19.43	19.48	19.34	19.29	19.55	19.67	19.44	19.42	19.98	19.66	12.83	12.98	13.14	12.91	13.18	13.48	13.27
CaO	0.61	0.57	0.62	0.56	0.56	0.58	0.51	0.57	0.58	0.62	0.54	22.07	22.88	21.94	22.75	21.85	20.06	22.62
Na_2O	d.l.	d.l.	d.l.	d.l.	d.l.	d.l.	d.l.	d.l.	d.l.	d.l.	d.l.	0.36	0.36	0.32	0.34	0.34	0.31	0.32
total	98.88	98.58	98.77	98.41	98.84	99.12	98.83	98.99	98.69	99.62	99.56	98.34	98.53	98.89	98.40	99.26	99.26	98.92
apfu																		
Si^{4+}	1.958	1.946	1.952	1.954	1.961	1.950	1.970	1.954	1.964	1.958	1.956	1.929	1.929	1.946	1.931	1.932	1.938	1.936
Ti^{4+}	0.004	0.003	0.003	0.002	0.002	0.002	0.002	0.002	0.002	0.002	0.003	0.009	0.008	0.006	0.007	0.008	0.007	0.006
Al^{3+}	0.043	0.040	0.038	0.045	0.038	0.039	0.034	0.039	0.037	0.037	0.039	0.082	0.077	0.068	0.077	0.079	0.075	0.070
Fe^{3+}	0.051	0.062	0.077	0.061	0.052	0.083	0.032	0.073	0.046	0.063	0.066	0.103	0.113	0.076	0.108	0.097	0.085	0.104
Fe^{2+}	0.780	0.774	0.764	0.775	0.792	0.762	0.781	0.772	0.785	0.751	0.768	0.223	0.189	0.246	0.199	0.236	0.299	0.203
Mn^{2+}	0.037	0.037	0.037	0.037	0.035	0.037	0.041	0.037	0.036	0.041	0.040	0.016	0.013	0.016	0.014	0.015	0.015	0.013
Mg^{2+}	1.116	1.115	1.123	1.118	1.110	1.124	1.127	1.119	1.118	1.138	1.124	0.734	0.740	0.746	0.738	0.747	0.765	0.754
Ca^{2+}	0.025	0.023	0.026	0.023	0.023	0.024	0.021	0.023	0.024	0.026	0.022	0.908	0.939	0.896	0.934	0.890	0.818	0.923
Na^{+}	0.000	0.000	0.000	0.000	0.000	0.000	0.000	0.000	0.000	0.000	0.00	0.027	0.027	0.023	0.025	0.025	0.023	0.024
Total	4.014	4.000	4.020	4.016	4.014	4.022	4.009	4.019	4.012	4.017	4.017	4.032	4.035	4.023	4.033	4.030	4.026	4.032
Wo%	1.31	1.22	1.34	1.22	1.21	1.25	1.08	1.22	1.24	1.33	1.16	48.67	50.24	47.43	49.93	47.52	43.47	49.12
En%	58.09	58.30	58.71	58.35	57.67	58.85	58.42	58.45	58.00	59.43	58.70	39.35	39.63	39.52	39.41	39.89	40.63	40.09
Fs%	40.60	40.47	39.95	40.43	41.12	39.91	40.49	40.33	40.76	39.23	40.14	11.97	10.13	13.05	10.66	12.59	15.91	10.79

Table 3. Representative electron microprobe analyses (EMPA) of pyroxene from the Bilwinowo IG-1 borehole (SAM); d.l. – below detection limit

sample	SiO_2	TiO_2	Al_2O_3	Fe_2O_3	MnO	MgO	CaO	Na_2O	K_2O	P_2O_5	LOI	Total	Mg#(1)	Fe#(2)	A/CNK(3)
	(%)														
B1-1127.5	42.73	3.66	16.05	18.24	0.27	4.48	8.30	2.84	0.67	1.05		98.30	0.21	0.79	1.36
B1-1336	49.79	2.90	14.81	14.33	0.24	3.44	7.89	2.72	1.69	0.99	1.01	99.81	0.21	0.79	1.20
B1-1601.5	43.65	3.46	15.28	17.06	0.25	4.34	8.66	2.88	1.06	1.13		97.77	0.22	0.78	1.21
B1-1953	42.29	4.10	14.70	19.95	0.29	4.73	9.26	2.44	0.57	1.07	0.2	99.67	0.21	0.79	1.20
B1-1980	43.33	3.88	15.45	18.98	0.28	4.63	8.81	2.57	0.65	1.01		99.67	0.21	0.79	1.28
JS-1225	45.34	2.41	16.48	15.46	0.21	4.07	8.57	3.28	0.63	0.59	1.27	98.31	0.23	0.77	1.32
JS-1229	47.08	2.13	16.83	15.43	0.32	5.38	8.65	3.21	0.56	0.50	0.31	100.40	0.28	0.72	1.36
U11-1515	40.56	4.34	14.27	20.20	0.33	5.25	8.56	2.59	0.57	1.43		98.10	0.22	0.78	1.22
U11-1515.8	41.34	3.80	15.05	19.55	0.30	4.80	8.94	2.72	0.57	1.46		98.54	0.21	0.79	1.23
U11-1518	41.48	4.18	14.63	20.71	0.32	4.95	9.51	2.45	0.50	1.26	-0.4	99.66	0.21	0.79	1.17
S1-843	45.36	2.18	16.50	16.49	0.25	6.10	9.22	2.39	0.47	0.43	0.31	99.70	0.29	0.71	1.37
S2-877	47.46	1.58	18.28	13.68	0.24	5.25	9.40	1.63	0.65	0.26	1.3	99.75	0.30	0.70	1.57
S2-1296A	43.66	1.84	12.87	22.66	0.40	7.84	5.76	2.17	0.76	0.47		98.42	0.28	0.72	1.48
S2-1296B	43.62	2.41	15.07	19.23	0.29	5.09	8.22	2.70	0.55	0.78		97.95	0.23	0.77	1.31
S2-1619	46.60	2.10	15.68	15.78	0.26	4.78	8.33	2.81	0.77	0.60		97.72	0.25	0.75	1.32
S2-1623	45.00	2.37	15.63	17.42	0.24	4.29	8.37	2.65	0.71	0.94		97.61	0.21	0.79	1.33

Table 4. Bulk-rock geochemistry (major elements) of the jotunites from the SAM and the Sejny Intrusion; (1) Mg# = MgO/(MgO+FeO); (2) Fe# = FeO/(MgO+FeO); (3) A/CNK = Al_2O_3/(CaO+Na_2O+K_2O)

sample	Y	La	Ce	Pr	Nd	Sm	Eu	Gd	Tb	Dy	Ho	Er	Tm	Yb	Lu	ΣREE	Eu/Eu*	La/Yb_n
	(ppm)																	
B1-1127.5	53.4	83.6	189.7	26.00	109.0	20.64	5.07	18.00	2.33	12.73	2.31	6.15	0.71	4.22	0.60	481.06	0.8	13.36
B1-1336	60.8	102.0	221.0	28.60	114.0	20.80	5.00	16.20	2.27	12.30	2.25	6.02	0.77	4.79	0.75	536.75	0.83	14.36
B1-1601.5	74.4	119.1	269.3	37.10	152.9	28.52	5.78	24.96	3.29	18.32	3.34	9.01	1.04	6.10	0.86	679.62	0.66	13.16
B1-1953	63.9	90.7	198.7	25.88	108.0	20.81	4.14	17.33	2.36	12.89	2.33	6.18	0.78	5.03	0.70	495.83	0.67	12.16
B1-1980	49.7	81.0	174.6	23.06	95.8	16.80	4.22	14.39	1.93	10.28	1.85	4.78	0.65	3.85	0.58	433.79	0.83	14.18
JS-1225	41.3	53.5	122.0	16.40	65.8	13.00	3.19	10.50	1.51	8.36	1.53	4.15	0.53	3.30	0.54	304.31	0.83	10.93
JS-1229	32.8	40.7	93.7	12.60	51.1	10.20	2.73	8.36	1.24	6.52	1.23	3.37	0.45	2.69	0.42	235.31	0.90	10.20
U11-1515	74.1	101.1	241.3	34.40	148.2	28.47	5.49	25.31	3.27	17.92	3.25	8.52	0.96	5.56	0.79	624.54	0.63	12.26
U11-1515.8	75.2	99.7	236.0	34.10	145.6	28.11	5.60	25.02	3.23	17.77	3.19	8.47	0.97	5.61	0.79	614.16	0.65	11.98
U11-1518	66.2	83.5	192.1	26.84	119.7	22.36	4.35	19.85	2.65	14.36	2.62	6.87	0.92	5.16	0.78	502.06	0.63	10.91
S1-843	23.4	20.8	46.4	6.27	26.3	5.46	1.95	5.05	0.81	4.47	0.92	2.51	0.34	2.16	0.35	123.79	1.14	6.49
S2-877	19.9	17.9	36.0	4.98	21.0	4.30	1.62	4.20	0.65	3.80	0.78	2.27	0.31	1.96	0.32	100.09	1.17	6.16
S2-1296B	31.3	40.3	90.6	12.3	53.3	10.52	2.75	9.26	1.27	7.16	1.33	3.61	0.43	2.59	0.37	235.79	0.85	10.49
S2-1619	33.6	35.6	79.5	10.70	45.6	9.48	2.96	8.86	1.27	7.34	1.41	3.93	0.50	3.13	0.45	210.73	0.99	7.67
S2-1623	38.8	43.4	118.2	16.60	70.6	13.55	3.32	11.90	1.56	8.70	1.61	4.40	0.52	3.12	0.44	297.92	0.80	9.38

Table 5. Bulk-rock geochemistry (Y + REE) of the jotunites from the SAM and the Sejny Intrusion

sample	Th	Zr	Hf	Nb	Ta	Rb	Sr	Ba	Cr	Ni	Co
	(ppm)										
B1-1336	3.01	367.0	6.9	33.4	1.36	23.0	488.0	1417	22	21	32.0
B1-1953	1.50	227.1	5.8	33.0	1.30	3.5	489.1	573	60	33	48.5
B1-1980	1.40	248.8	6.2	25.7	1.20	4.5	555.6	623	70	33	46.0
JS-1225	1.22	246.0	5.1	15.8	0.66	4.0	489.0	677	22	30	41.0
JS-1229	1.38	176.0	3.6	16.7	0.81	3.0	474.0	380	36	38	42.0
U11-1518	1.80	269.3	7.1	29.5	1.40	4.3	513.0	346	50	32	45.7
S1-843	0.12	59.0	1.5	6.2	0.22	2.0	523.0	427	69	72	52.0
S2-877	0.20	56.9	1.5	5.0	0.20	11.4	446.3	400	90	79	44.6

Table 6. Bulk-rock geochemistry (trace elements) of the jotunites from the SAM and the Sejny Intrusion

PETROGRAPHY

According to Streckeisen (1974), jotunites are hypersthene monzodiorites or monzonorites. They are common components of the SAM and the Sejny Intrusion, appearing as chilled margins and dykes crosscutting anorthosites and surrounding zones of norite or gabbro rocks. The original melt character of the jotunites is supported by their chilled microtextures. Jotunites show characteristic medium- to fine-grained textures (Text-fig. 2A, B) of chilled type melts, which suggests a later injection of hot jotunitic magma into mafic rocks. They appear as dykes that result in a directional texture, which is additionally underlined by porphyritic, very often kinked plagioclase crystals (Text-fig. 2C, D). However, jotunites from the Sejny Intrusion contain more porphyritic plagioclase than those from the Bilwinowo IG-1 borehole. The jotunite dykes are holocrystalline.

Petrographically, the jotunites are made up of andesine or labradorite (antiperthitic) plagioclase, Ca-rich pyroxene, Ca-poor pyroxene (Text-fig. 2C), Fe-Ti oxides (magnetite and ilmenite), prismatic, elongate apatite crystals (Text-fig. 2E) up to 0.25 mm long as irregular inclusions in groundmass plagioclase, and traces of brownish Ti-rich (up to 4.8 wt. %) biotite or amphibole after pyroxene. Zircon and baddeleyite are accessory minerals. In the most evolved type of jotunites, microperthitic K-feldspar coexists with plagioclase. Fe-Ti oxide minerals are commonly interstitial with amoeboidal shapes (Text-fig. 2B). In some chilled rocks, Fe-Ti oxides occur as small rounded grains associated with mafic minerals; pyroxene and biotite.

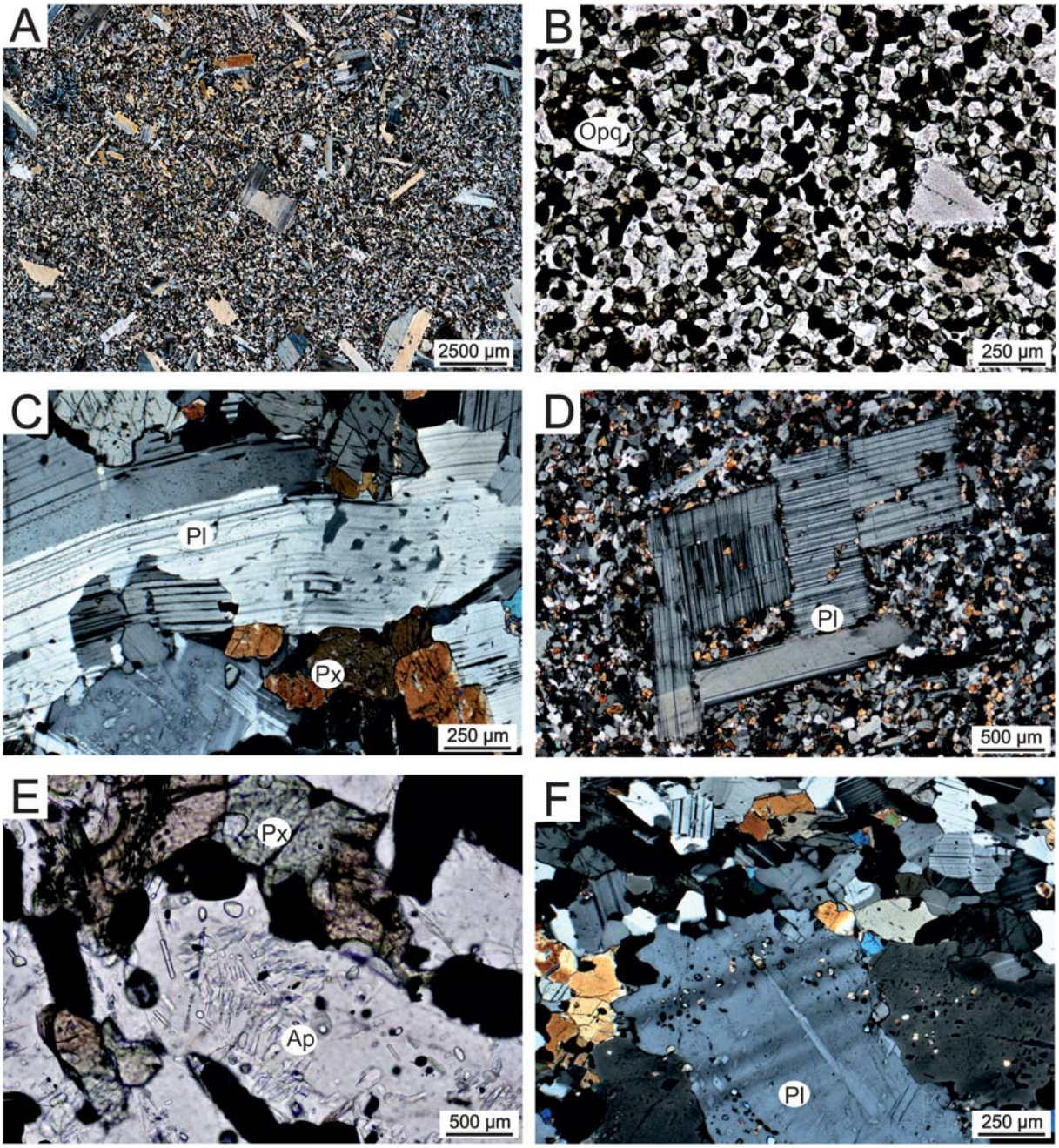

Text-fig. 2. Microphotographs of: characteristic texture of porphyritic jotunite (A); Fe-Ti oxides (interstitial or amoeboidal in shape) associated with mafic pyroxene (B); cambered plagioclase megacrysts with curved twin planes as evidence of diapiric emplacement of anorthosite crystal mush (C); plagioclase megacrysts within fine-grained groundmass (D); apatite prismatic microcrysts included in feldspars (E); fine-grained jotunite and plagioclase megacryst with small pyroxene and oxide grains that possibly result from the crystallization of melt inclusions (F). Ap – apatite, Opq – opaque minerals, Pl – plagioclase, Px – pyroxene

Tabular crystals of plagioclases, both in the groundmass and porphyritic ones, are the main rock-forming minerals. Some megacrysts, up to 5 mm long, show kinked twin planes, which were considered evidence for the diapiric emplacement of crystal mush (Wiszniewska *et al*. 2002; Wiszniewska and Petecki 2014; Text-fig. 2C). Megacrysts of plagioclase do not show zonation, but do show slight

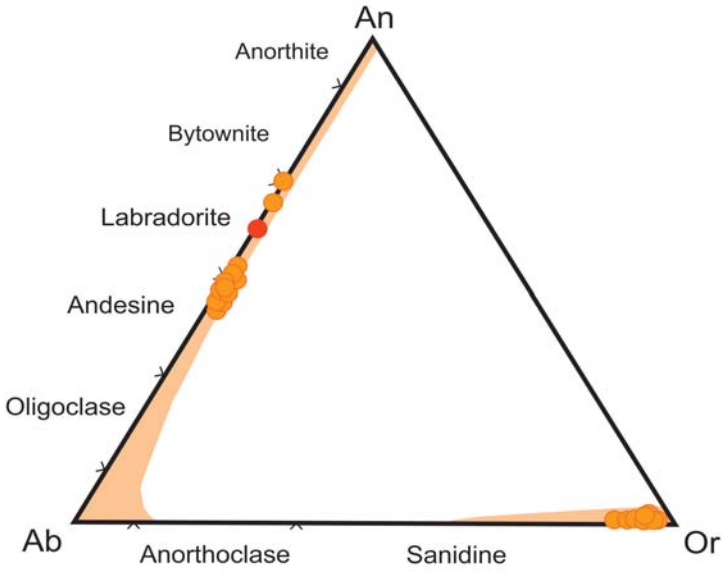

Text-fig. 3. Ternary plot of Bilwinowo IG-1 feldspar compositions and antiperthitic exsolutions (orange circles) compared to average composition of Sejny feldspars (red circle). The stability fields of feldspars, at a pressure of 4–5 kbar (400–500 MPa) and temperature of c. 500ºC, are marked as light-orange fields (based on Nekvasil and Burnham 1987)

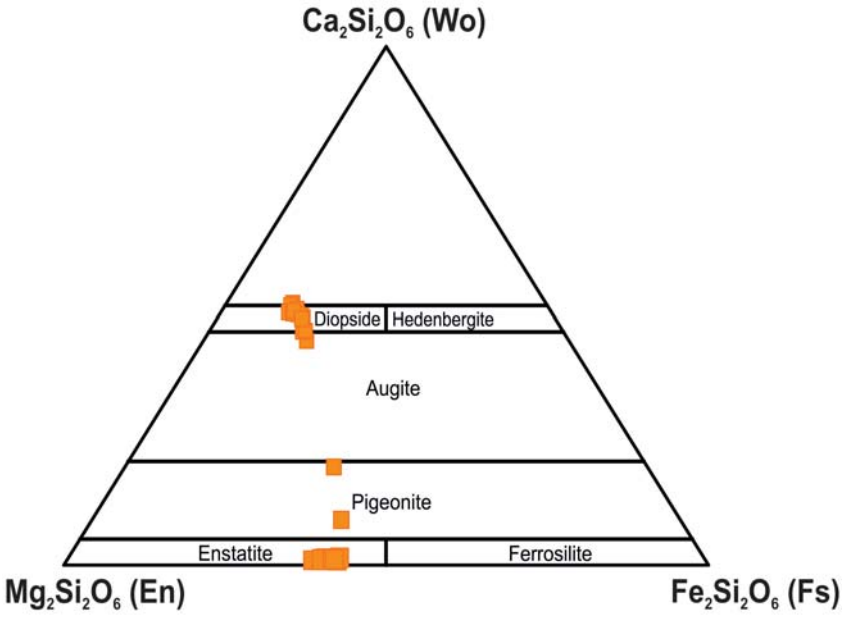

Text-fig. 4. Ternary plot of Bilwinowo IG-1 pyroxene compositions (orange squares)

differences in composition in each massif, with an average of $An_{48(45–52)}$ in the Bilwinowo IG-1 borehole and $An_{60(51–61)}$ in the Sejny Intrusion (Gawęda *et al.* 2009; Table 1; Text-fig. 3). Plagioclase, with a more anorthitic composition up to An_{74}, was also found in the rock groundmass. The plagioclase megacrystals are filled with needles of Fe-Ti oxides. Locally, they also contain an association of very small pyroxene and ore-oxide grains that possibly resulted from the crystallization of melt inclusions. These inclusions appear parallel to the crystals rims (Text-fig. 2F). Antiperthitic exsolutions of orthoclase composition

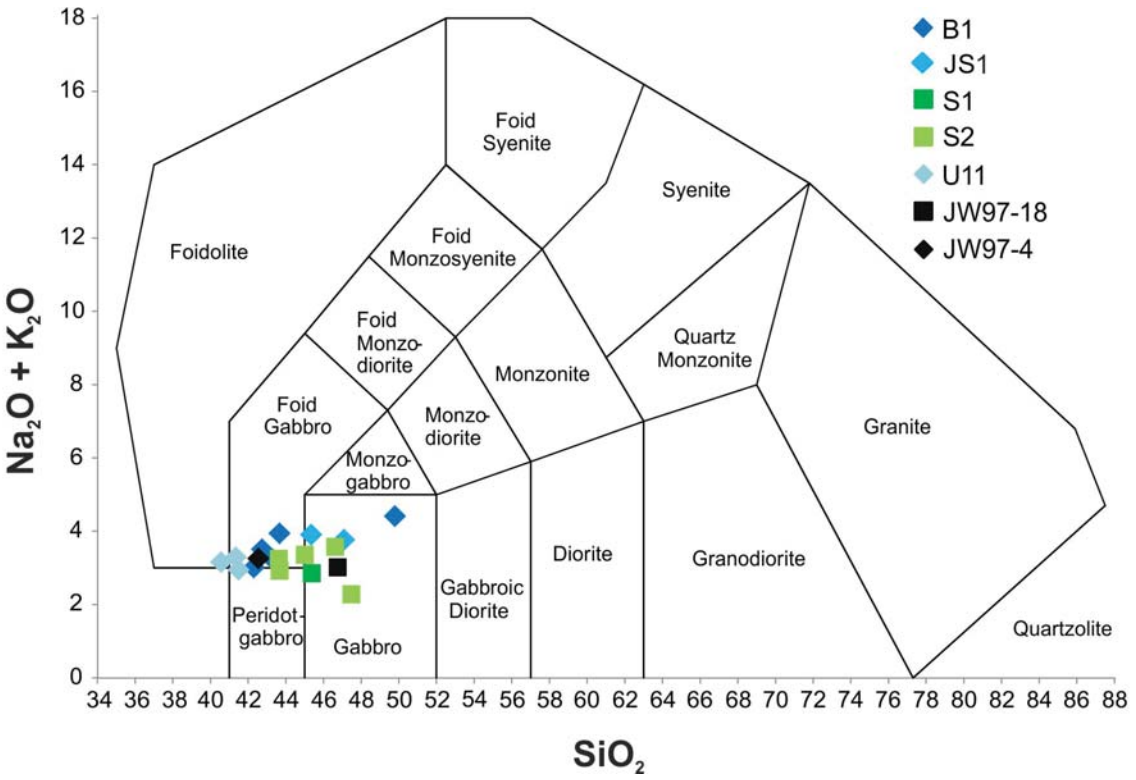

Text-fig. 5. Position of Polish jotunites in the TAS plutonic diagram Na_2O+K_2O *vs.* SiO_2, after Middlemost (1994). B1 – Bilwinowo IG-1, JS1 – Jezioro Szlinokiemskie IG-1, S1 – Sejny IG-1, S2 – Sejny IG-2, U11 – Udryń 11; JW97-18 and JW97-4 after Wiszniewska *et al.* (2002)

($Or_{96}Ab_4$) are also very common (Table 2). At a pressure of 4–5 kbar (400–500 MPa) – corresponding to the depth of the anorthosite diapir final emplacement – calculated equilibrium temperatures for feldspars oscillate around 500ºC (Nekvasil and Burnham 1987). Stability fields of feldspars can be seen in Text-fig. 3.

Pinkish to pinkish green orthopyroxene and colourless to brownish clinopyroxene (Text-fig. 2C, E) form anhedral grains up to 0.5 mm, and sporadically up to 1 mm long. The content of Ca-rich ($En_{40}Fs_{16}Wo_{48}$; mg# = 71) and Ca-poor ($En_{58}Fs_{40}Wo_2$; mg# = 57) pyroxene (Table 3; Text-fig. 4) in jotunites from the Bilwinowo IG-1 borehole are almost equal, with a slight dominance of Ca-poor pyroxene. As in plagioclase, pyroxene shows differences in composition in the Bilwinowo IG-1 and Sejny IG-1 and IG-2 boreholes, with moderately low Ca content both in Ca-poor and Ca-rich pyroxene (mg# = 59 and 75, respectively) in jotunites from the Sejny IG-1 and IG-2 boreholes (Gawęda *et al.* 2009). Numerous Schiller lamellae of Ca-poor pyroxene are a characteristic feature of Ca-rich pyroxene crystals: this kind of exsolution does not occur in Ca-poor pyroxene (orthopyroxene). At the contact with younger, granitoid dykes, pyroxene is occasionally replaced to various degrees by green amphibole. Ilmenite and magnetite are the main opaque minerals, but sulphides such as pyrrhotite and pyrite after pyrrhotite are also present, although less abundant. K-feldspar is a rare mineral and occurs as interstitial grains of irregular shape, or more often as antiperthitic exsolutions in plagioclase.

GEOCHEMISTRY

Samples from the Hidra Massif (HM) and the Bjerkreim-Sokndal Layered Intrusion (BSLI) in the Rogaland Province (c. 930–920 Ma), SW Norway (Demaiffe and Hertogen 1981; Schärer *et al.* 1996; Vander Auwera *et al.* 1998) and the Korosten Complex (KC-J – jotunite; KC-QJ – quartz jotunite), Ukraine (1.8 Ga; Duchesne *et al.* 2017; Shumlyanskyy *et al.* 2017) have been used for geochemical comparison with the Polish jotunites.

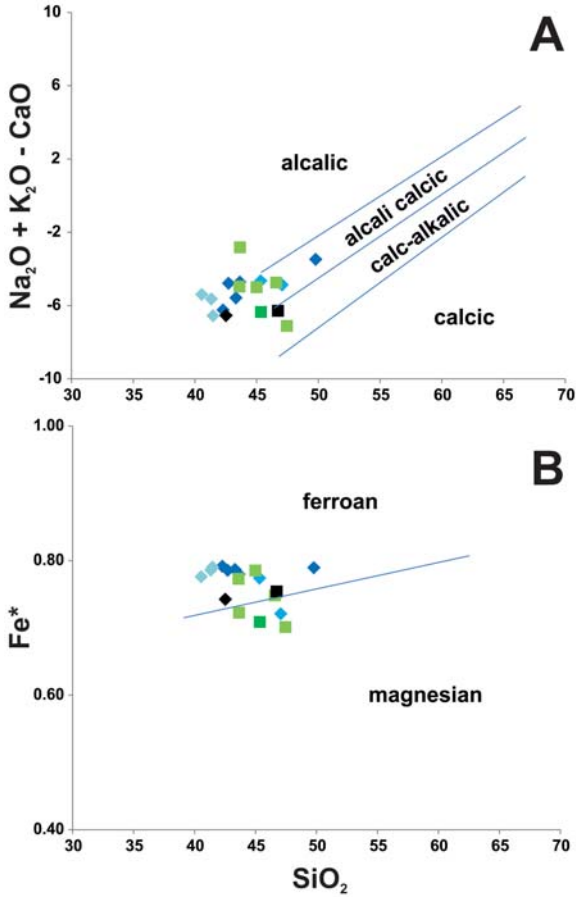

Text-fig. 6. Composition of Polish jotunites on various plots. A – Na_2O+K_2O-CaO *vs*. SiO_2 after Frost *et al.* (2001); B – Fe* (FeO_t/MgO) *vs*. SiO_2 (wt %) after Frost *et al.* (2001); data in Table 4. See Text-fig. 5 for explanation of symbols

Major elements

The major element compositions of the samples are given in Table 4. Jotunites with an A/CNK index (Aluminous Saturation Index) from 1.17 to 1.48 are metaluminous. Based on the TAS (total alkalis-silica) discrimination diagram for plutonic rocks (Middlemost 1994; Text-fig. 5), jotunites are placed in the fields of gabbro, peridotite–gabbro and foid–gabbro. Most samples are calc-alkalic to alkali calcic, with minor alkalic, and ferroan components following Frost's classification (Frost *et al.* 2001; Text-fig. 6). Samples from the SAM show less diversity on Frost's diagram and are only alkali calcic. Samples from the Sejny Intrusion are generally slightly less ferroan. The same regularity can be seen in the Mg# and Fe# indexes (Table 4) and on Harker diagrams (Text-fig. 7C). Variation diagrams, as a function of Mg# (Text-fig. 8D), show increased amounts of SiO_2 with an increase in Mg#, which is caused by a faster decrease of Fe_2O_3 than MgO with SiO_2 increase. Jotunites define trends of decreasing Fe_2O_3, TiO_2, P_2O_5 and MgO with increasing SiO_2 on Harker diagrams (Text-fig. 7C–F). In general, the Bilwinowo IG-1 and Udryń 11 jotunites follow less dispersed trends among all samples, whereas the Sejny IG-1 and IG-2 samples are rather scattered; the jotunites from Jezioro Szlinokiemskie IG-1 have an intermediate pattern. Jotunites from anorthosite massifs within the Mazury Complex can be divided into two groups on the basis of chemical composition. It is clearly visible on both the Harker (Text-fig. 7C, E, F) and Mg# diagrams (Text-fig. 8C, E, F) that jotunites from the SAM have higher amounts of TiO_2 (up to 4.34 wt. %), Fe_2O_3 (up to 20.71 wt. %) and P_2O_5 (up to 1.46 wt. %) than those from the Sejny Intrusion (Table 4). TiO_2 and P_2O_5 peak at c. Mg# = 20, reflecting saturation in Ti-rich oxide minerals and apatite. Three samples (B1-1336, S2-1296A, S2-877) deviate from the trends. Sample B1-1336 has higher SiO_2 and K_2O contents and lower TiO_2 and Fe_2O_3 contents, and is located close to the sample from the Bjerkreim-Sokndal Intrusion (referred to as a primitive jotunite). Sample S2-1296A is rich in Fe_2O_3 and MgO but depleted in CaO and SiO_2, suggesting enrichment in orthopyroxene with minor clinopyroxene. Sample S2-877 has a high Al_2O_3 content, which may reflect the abundance of plagioclase; however, it has a very low content of Na and additionally an elevated content of Ca and SiO_2, which may indicate the presence of clinopyroxene.

Samples from the Hidra Massif and the Bjerkreim-Sokndal Intrusion (interpreted as primitive jotunite) are quite similar to the Sejny Intrusion jotunites in terms of Fe_2O_3 and P_2O_5 content, and to the SAM jotunites based on TiO_2 values. However, jotunites from Rogaland are visibly enriched in SiO_2 and alkalis. Jotunites from the Korosten Massif have also higher levels of Na and K (Text-fig. 8G, H).

Trace elements

In general, REE contents are inversely correlated with SiO_2 and with Mg# (Text-fig. 9), reaching a maximum at c. Mg# = 20. Jotunites from the Sejny Intrusion with higher SiO_2 have lower REE contents, with ΣREE up to 298 ppm, in contrast to 680 ppm in the Bilwinowo IG-1 samples. Jotunites can be sub-divided into two groups based on Eu/Eu* values (Text-fig. 10), where Eu anomalies are either slightly negative, positive or even absent (e.g.,

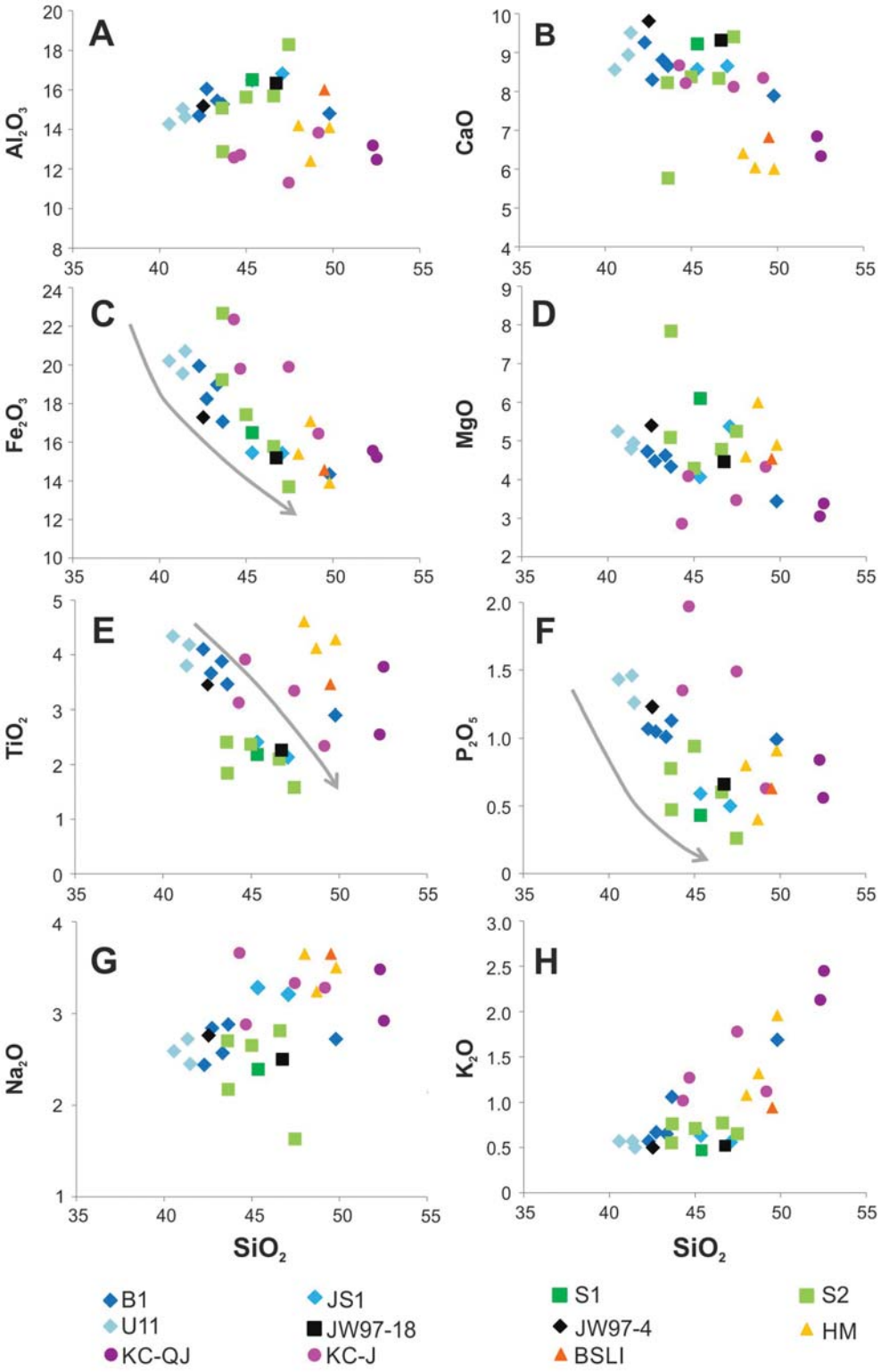

Text-fig. 7. Harker variation diagrams of Polish jotunites compared to the jotunites from the Hidra Massif, the Bjerkreim-Sokndal Layered Intrusion (Rogaland Province, Norway) and the Korosten Complex (Ukraine); see Table 4 for data on Polish jotunites. B1 – Bilwinowo IG-1, JS1 – Jezioro Szlinokiemskie IG-1, S1 – Sejny IG-1, S2 – Sejny IG-2, U11 – Udryń 11; JW97-18 and JW97-4 after Wiszniewska *et al.* (2002); HM – Hidra Massif (see Demaiffe and Hertogen 1981); KC-QJ – Korosten Complex (quartz jotunite); KC-J – Korosten Complex (jotunite; see Duchesne *et al.* 2017); BSLI – Bjerkreim-Sokndal Layered Intrusion (see Vander Auwera *et al.* 1998)

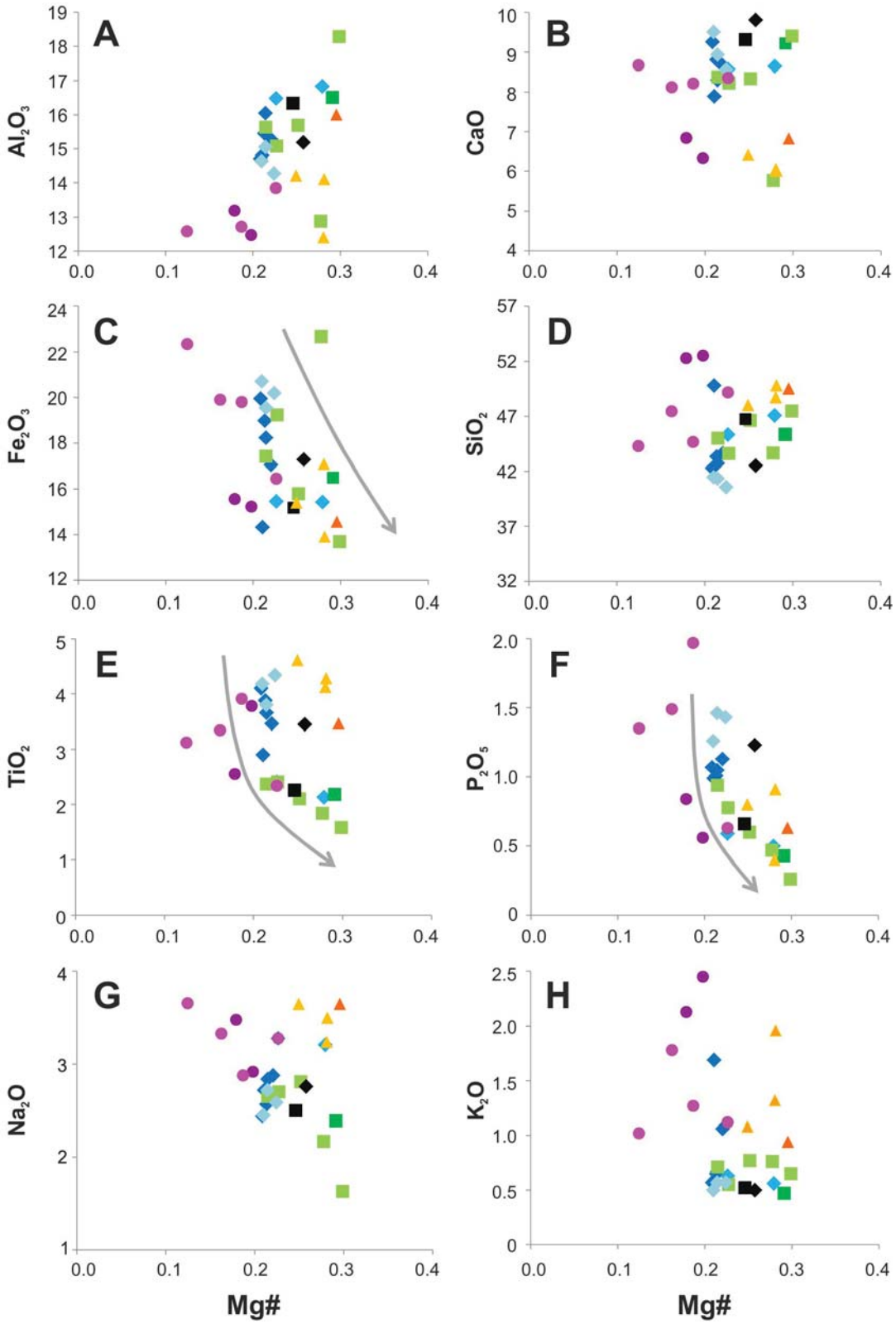

Text-fig. 8. Major element composition of Polish jotunites as a function of Mg# (MgO/(MgO +FeO_t)), compared to the jotunites from the Hidra Massif, the Bjerkreim-Sokndal Layered Intrusion (Rogaland Province, Norway) and Korosten Complex (Ukraine); see Table 4 for data on Polish jotunites. See Text-fig. 7 for explanation of symbols

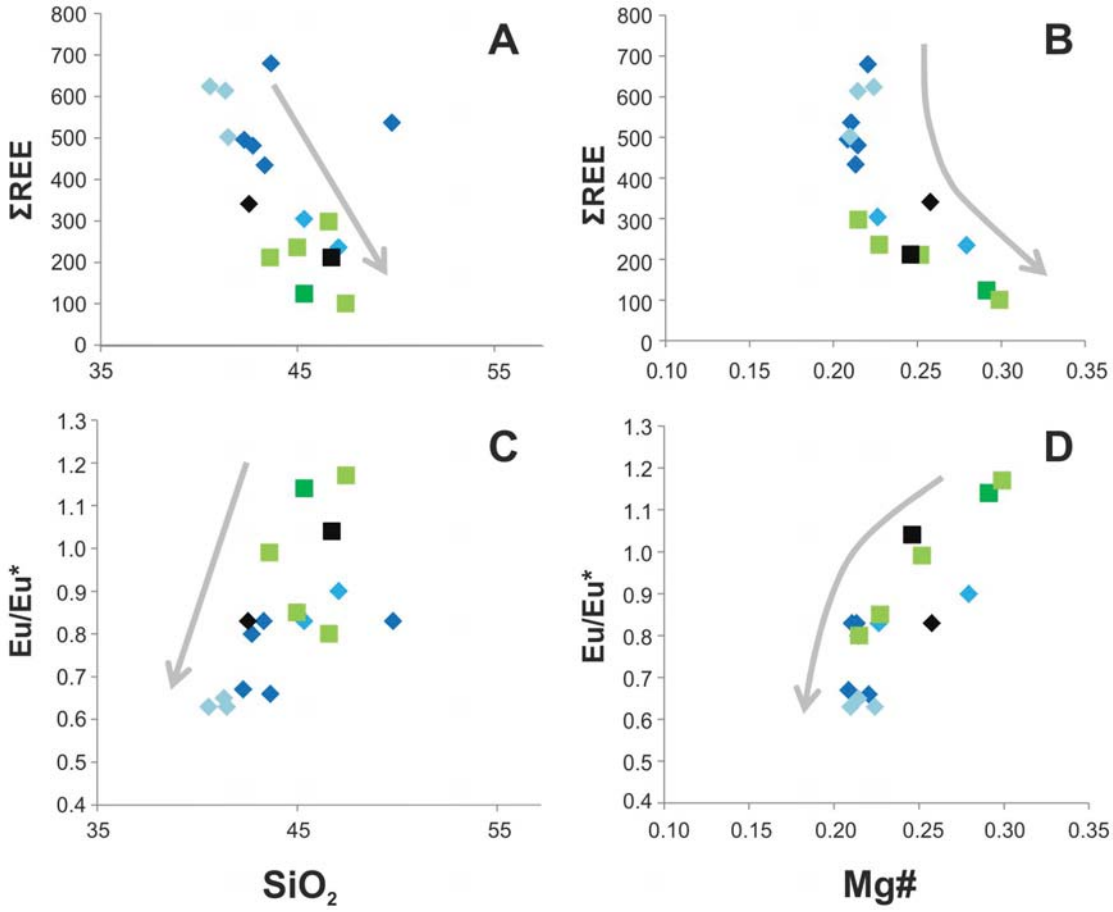

Text-fig. 9. Sum of REE and Eu/Eu* in jotunites as a function of SiO_2 and Mg# (MgO/(MgO +FeO_t)); data in Table 5. See Text-fig. 5 for explanation of symbols

S2-1619). Eu/Eu* ratios for the Sejny Intrusion jotunites (with higher SiO_2 contents) range from 1.17 to 0.8, but for the SAM samples decrease from about 0.83 for Bilwinowo IG-1 down to 0.63 for Udryń 11 (Table 5; Text-fig. 10). The $[La/Yb]_N$ ratio (Table 5) remains at relatively moderate values for the SAM jotunites (averaging 12.25±2) to low values for the Sejny Intrusion jotunites (averaging 8.68 ± 3).

On a multi-element diagram (Table 6; Text-fig. 10), the Sejny Intrusion jotunites have distinctly lower contents of Rb, Th, Nb, Ta, Zr and Hf, whereas the SAM jotunites do not show negative anomalies. Noteworthy, the amount of Sr is constant for the SAM and Sejny Intrusion jotunites, but the SAM pattern shows a prominent negative anomaly, suggesting extensive crystallization of plagioclase (Vander Auwera *et al.* 1998). Interestingly, the Sejny Intrusion jotunites show a relatively small excess in P, whereas the SAM samples show a slight depletion in P.

DISCUSSION

Variation diagrams, multi-element diagrams, and other geochemical data for jotunites from the boreholes in the SAM (Bilwinowo IG-1, Udryń 11 and Jezioro Szlinokiemskie IG-1) and Sejny Intrusion (Sejny IG-1 and Sejny IG-2) show slight differences in jotunite composition between the two massifs and can be subdivided into two groups. As proposed by Wiszniewska *et al.* (2002) on the basis of JW97-18 and JW97-4 samples, the Sejny Intrusion jotunites can be referred to as primitive (and similar to the Rogaland jotunites), whereas the SAM jotunites are more evolved.

Jotunites are characterised by very high contents of Fe, Ti and P (Vander Auwera *et al.* 1998). In the SAM, these elements are enriched (TiO_2, 2.13–4.34 wt. %; Fe_2O_3, 14.33–20.71 wt. %; and P_2O_5, 0.5–1.46 wt. %), compared to the Sejny Intrusion (TiO_2, 1.58–2.41 wt. %; Fe_2O_3, 13.68–19.23 (up to 22.66) wt. %;

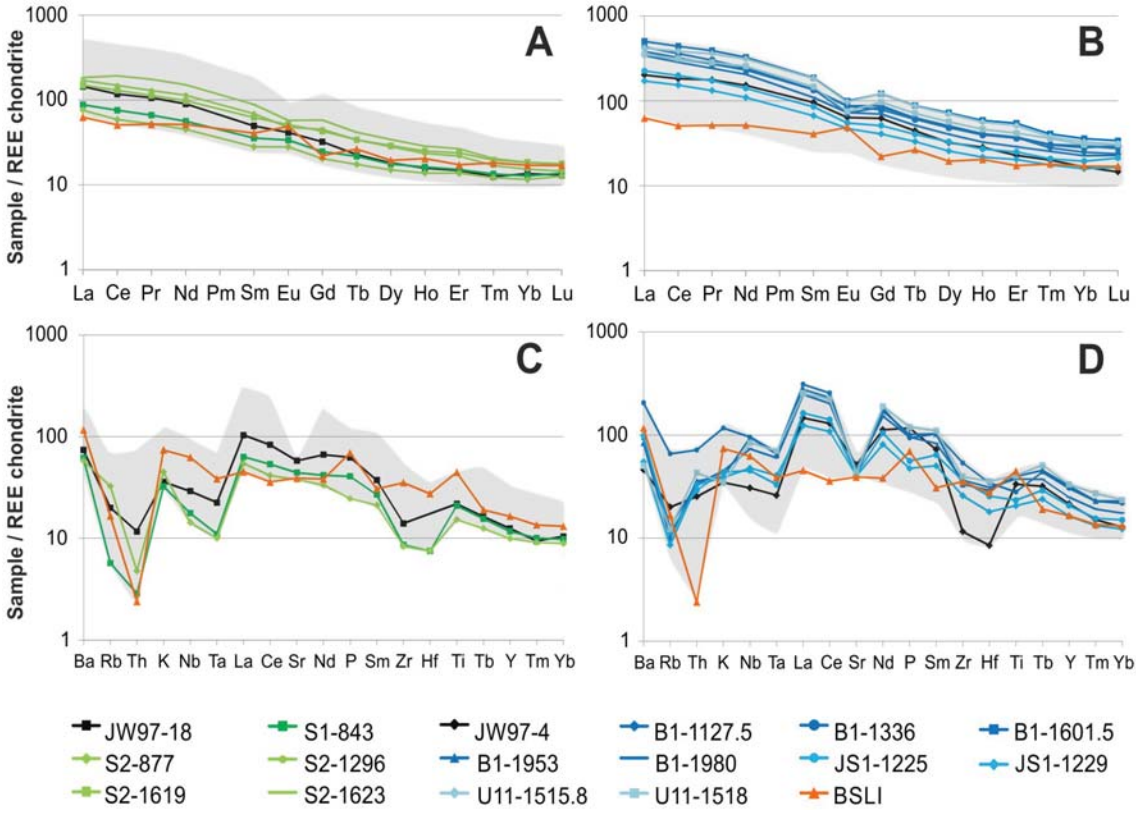

Text-fig. 10. Chondrite normalised REE diagram (A and B) and trace element spidergrams (C and D) for the SAM and Sejny Intrusion jotunites compared to the Bjerkreim-Sokndal primitive jotunites (Vander Auwera *et al.* 1998). Normalising values from Boynton (1984) and Thompson *et al.* (1982); data in Tables 5 and 6

and P_2O_5, 0.26–0.94 wt. %) (Table 4). According to Vander Auwera *et al.* (1998), compositions poor in P_2O_5, as in the Sejny Intrusion, are referred to as 'primitive' to distinguish them from 'evolved' jotunites. Primitive and more evolved jotunites are common in other massifs in the Rogaland Province (e.g., Hidra Massif; see Demaiffe and Hertogen 1981).

The Sejny Intrusion jotunites show limited variations in the K_2O content, whereas the SAM jotunites display considerable variability in this element (Text-figs 7 and 8), which may be caused by variable degree of contamination by the surrounding host rocks during diapiric emplacement. Additionally, the SAM rocks composition indicates their more evolved character. Jotunites show distinct differentiation in the SiO_2 content, with 43.62–47.46 wt. % for the Sejny Intrusion primitive jotunites and 40.56–47.08 wt. % for the SAM evolved jotunites (Table 4). Relatively low SiO_2 contents were also reported from the Korosten Anorthosite-Norite Complex (see sample K-12 in Duchesne *et al.* 2017). Primitive jotunite from BSLI has a high SiO_2 content (49.50 wt. %) as indicated by sample B1-1336 only (49.79 wt. %).

According to Vander Auwera *et al.* (1998), primitive jotunites are depleted in Ta (but not in Nb) and Hf (but not in Zr) relative to the neighbouring REE, whereas Ti shows a small excess. Although the Sejny Intrusion jotunites referred to here as primitive reveal strong depletions in Ta and Hf, their depletions in Nb and Zr are also remarkable (Text-fig. 10). The Sejny Intrusion jotunites show an excess in Ti. Along the path of progressive differentiation from the Sejny Intrusion to the SAM jotunites, a relative depletion of Ti appears, while the relative depletion in Hf and Zr become less pronounced, indicating crystallization of Fe-Ti oxides. All evolved jotunites are clearly depleted in Sr relative to Ce and Nd (Text-fig. 10), which is related to extensive crystallization of plagioclase. Small relative depletions in P, or lack of a phosphorus anomaly in the SAM jotunites, are not characteristic of evolved jotunites, which are usually rich in apatite compared to mangerites (Text-fig. 10). Relatively low

SiO_2 contents (Table 4) of the SAM rocks preclude terming them as mangerites. Interestingly, a notable difference appears in the Eu/Eu* evolution: there is a clear increase in the negative Eu anomaly with a decrease in Mg# (Text-fig. 9), which can be explained by a later saturation in apatite that delayed its buffering effect on plagioclase subtraction (Duchesne *et al.* 2017). Thorium shows a huge depletion against REE in the primitive Sejny Intrusion jotunites, which is not present in the SAM rocks (Text-fig. 10). Lower amounts of total REE and low values of $[La/Yb]_N$ (Table 5) for the Sejny Intrusion jotunites additionally support their primitive character. It is worth noting that sample locations on diagrams from the Jezioro Szlinokiemskie IG-1 borehole (SAM; samples JS-1225 and JS-1229) are close to sample locations from the Sejny Intrusion and suggest a continuous transition in chemical composition between the Sejny Intrusion and SAM jotunites.

The same regularity is marked by plagioclase and pyroxene compositions in jotunites from the Bilwinowo IG-1, Sejny IG-1 and Sejny IG-2 boreholes. Due to the slightly more anorthitic character of plagioclase in the Sejny Intrusion jotunites and pyroxene richer in Fe in the Bilwinowo IG-1 rocks (which affects the Fe content in the bulk-rock composition), the Sejny Intrusion jotunites can be treated as primitive.

Petrographic features of the jotunites studied, typical of chilled rocks at the margins of anorthosite massifs, are similar to those observed in the Hidra pluton in the Rogaland Province (Demaiffe and Hertogen 1981). These observations have led us to the conclusion that a liquid state existed. The mechanism of its formation may be similar to that of the Rogaland liquid line of descent (LLD). The Rogaland LLD was characterised based on a series of rocks occurring in forms of dykes at the marginal part of anorthosite intrusions like jotunites (hypersthene monzonites), mangerites (hypersthene quartz monzonites) and finally charnockites (hypersthene granites). The original liquid character of jotunites is confirmed by their microtexture. The evolution of the Rogaland LLD from 'primitive' jotunites up to charnockites was experimentally confirmed (Vander Auwera and Longhi 1994; Vander Auwera *et al.* 1998). Text-figs 7 and 8 show that samples from SAM and Sejny Intrusion plot close to those of the Rogaland intrusions and the Korosten Massif, where the LLD was studied (Duchesne *et al.* 2017). Moreover, the chondrite normalized REE distribution (Text-fig. 10) for Sejny rocks shows their affinity to BSLI primitive jotunites, which can be proven to have a similar character as the Sejny Intrusion jotunites. An overall resemblance can also be noted in the multi-element spidergrams (Text-fig. 10). The fractionation process could then lead to more evolved jotunites. On the other hand, charnockites were also found in the SAM (Bagiński *et al.* 2007), which additionally confirms a continuous transition to more silica-rich rocks. Rock evolution could involve some crustal contamination on its way to the surface. The general resemblance of the Polish jotunites with those from Rogaland once more may be evidence that they have been produced as a result of the same mechanism from a similar composition gabbronoritic crustal source (Duchesne *et al.* 2017), which is additionally supported by Sm/Nd and Re/Os isotopic data.

It is worth noting that jotunites in the form of chilled margins have been determined as 'primitive', and these in the form of dykes as 'evolved' (Vander Auwera *et al.* 1998), which matches the Polish jotunites – chilled margins occur in the jotunites from the Sejny Intrusion, and jotunitic dykes are present in the SAM.

CONCLUSIONS

Variations in mineral and whole-rock compositions indicate the presence of primitive jotunites in the Sejny Intrusion and evolved jotunites in the Suwałki Anorthosite Massif. They also point to a different evolution of the two massifs: either the SAM and the Sejny Intrusion jotunites came from two different magma chambers or, more convincingly, the jotunitic melts came from one magma chamber and their separation took place at a later stage, due to the fact that the Mazury Complex was created as a result of bimodal, multistage magmatism. It was stressed by Charlier *et al.* (2009) that individual differentiation trends for the Krzemianka and Udryń ore deposits in the SAM indicate that different parental magmas may have involved, and thus that the SAM is a composite pluton. The complexity of the SAM is indicative of its multistage formation and evolution of two or more influxes of magma into the emplacement level. Subsequent additional processes led to the formation of more evolved jotunitic magma in the SAM compared to the Sejny Intrusion.

Petrographic features of the jotunites, typical of chilled rocks with microtexture, at the margins of anorthosite massifs led to the conclusion about the liquid character of the jotunitic melt and evolution of the liquid line of descent (LLD) from 'primitive' jotunites up to charnockites.

On the basis of melting experiments on gabbroic rocks from the Harp Lake Massif, Labrador, and

the Rogaland jotunites under anhydrous conditions and at low to intermediate pressure (from 0.1 MPa to 1300 MPa), performed by Vander Auwera *et al.* (1998), it has been shown that melts of jotunitic composition can be parental to anorthosites. In view of their petrological and geochemical characteristics, the SAM and Sejny Intrusion jotunites are considered as possible candidates for the anorthosite source rocks in both massifs.

Acknowledgements

The authors would like to thank the journal reviewers, Profs. A. Gawęda and L. Shumlyanskyy, for their constructive criticism and helpful comments to the manuscript. Many thanks are expressed to Prof. A. Gawęda for her help in determining the feldspar stability fields, and to Prof. R. Macdonald and Jordan Todes for linguistic correction of the text.

REFERENCES

Ashwal, L.D. 1982. Mineralogy of mafic and Fe-Ti oxide-rich differentiates of the Marcy anorthosite massif, Adirondacks, New York. *American Mineralogist*, **67**, 14–27.

Ashwal, L.D. 1993. Proterozoic Massif-Type Anorthosites. In: Ashwal, L.D. (Ed.), Anorthosites, pp. 82–218. Springer Verlag; Heidelberg and New York.

Ashwal, L.D. 2010. The temporality of anorthosite. *The Canadian Mineralogist*, **48**, 711–728.

Bagiński, B., Duchesne, J.C., Vander Auwera, J., Martin, H. and Wiszniewska, J. 2001. Petrology and geochemistry of rapakivi-type granites from the crystalline basement of NE Poland. *Geological Quarterly*, **45**, 33–52.

Bagiński, B., Duchesne, J.C., Martin, H. and Wiszniewska, J. 2007. Isotopic and geochemical constraints on the evolution of the Mazury granitoids, NE Poland. In: Kozłowski, A. and Wiszniewska, J. (Eds), Granitoids in Poland, pp. 11–30. AM Monograph No. 1, University of Warsaw; Warszawa.

Boynton, W.V. 1984. Cosmochemistry of the rare earth elements: meteorite studies. In: Henderson, P. (Ed.), Rare Earth Element Geochemistry, 63–114. Elsevier; Amsterdam.

Charlier, B., Namur, O., Duchesne, J.C., Wiszniewska, J., Parecki, A. and Vander Auwera, J. 2009. Cumulate origin and polybaric crystallization of Fe-Ti oxide ores in the Suwałki anorthosite, northeastern Poland. *Economic Geology*, **104**, 205–221.

Cieśla, E., Podemski, M., Ryka, W. and Wybraniec, S. 1998. Outline studies of the Suwałki Anorthosite Massif. In: Ryka, W. and Podemski, M. (Eds), Geology of the Suwałki Anorthosite Massif (northeastern Poland). *Prace Państwowego Instytutu Geologiczego*, **61**, 39–45.

Claesson, S., Bogdanova, S.V., Bibikova, E.V. and Gorbatschev, R. 2001. Isotopic evidence for Palaeoproterozoic accretion in the basement of the East European Craton. *Tectonophysics*, **339**, 1–18.

Cymerman, Z. 2014. Structural and kinematic analysis and the Mesoproterozoic tectonic evolution of the Suwałki Massif and its surroundings (NE Poland). *Prace Państwowego Instytutu Geologicznego*, **201**, 1–172. [In Polish]

Demaiffe, D. and Hertogen, J. 1981. Rare earth element geochemistry and strontium isotopic composition of a massif-type anorthositic-charnockitic body: the Hidra Massif (Rogaland, SW Norway). *Geochimica et Cosmochimica Acta*, **45**, 1545–1561.

Droop, G.T.R. 1987. A general equation for estimating Fe^{3+} concentrations in ferromagnesian silicates and oxides from microprobe analyses, using stoichiometric criteria. *Mineralogical Magazine*, **51** (361), 431–435.

Duchesne, J.C. and Demaiffe, D. 1978. Trace elements and anorthosite genesis. *Earth and Planetary Science Letters*, **38**, 249–272.

Duchesne, J.C., Liégeois, J.P., Vander Auwera, J. and Longhi, J. 1999. The crustal tongue melting model and the origin of massive anorthosites. *Terra Nova*, **11**, 100–105.

Duchesne, J.C., Martin, H., Bagiński, B., Wiszniewska, J., and Vander Auwera, J. 2010. The origin of ferroan-potassic A-type granitoids: the case of the hornblende-biotite granite suite of the Mesoproterozoic Mazury complex, northeastern Poland. *The Canadian Mineralogist*, **48**, 947–968.

Duchesne, J.C., Roelandts, I., Demaiffe, D., Hertogen, J., Gijbels, R. and De Winter, J. 1974. Rare-earth data on monzonoritic rocks related to anorthosites and their bearing on the nature of the parental magma of the anorthositic series. *Earth and Planetary Science Letters*, **24**, 325–335.

Duchesne, J.C., Shumlyanskyy, L. and Mytrokhyn, O.V. 2017. The jotunite of the Korosten AMCG complex (Ukrainian shield): Crust or mantle derived? *Precambrian Research*, **299**, 58–74.

Emslie, R.F. 1975. Pyroxene megacrysts from anorthositic rocks; new clues to the sources and evolution of the parent magmas. *The Canadian Mineralogist*, **13**, 138–145.

Emslie, R.F. 1978. Anorthosite massifs, Rapakivi granites, and the late Proterozoic rifting of North America. *Precambrian Research*, **7**, 61–98.

Emslie, R.F. 1985. Proterozoic anorthosite massifs. In: Tobi, A.C. and Touret, J.L.R. (Eds), The deep Proterozoic Crust in the North Atlantic Provinces, pp. 39–60. NATO ASI Series (Series C: Mathematical and Physical Sciences), vol. 158. Springer; Dordrecht.

Emslie, R.F., Hamilton, M.A. and Thériault, R.J. 1994. Petrogenesis of a mid-Proterozoic anorthosite-mangerite-charnockite-granite (AMCG) complex: Isotopic and chemical evidence from the Nain Plutonic Suite. *The Journal of Geology*, **102**, 539–558.

Fram, M.S. and Longhi, J. 1992. Phase equilibria of dikes associated with Proterozoic anorthosite complexes. *American Mineralogist*, **77**, 605–616.

Frost, B.R., Barnes, C.G., Collins, W.J., Arculus, R.J., Ellis, D.J. and Frost, C.D. 2001. A geochemical classification for granitic rocks. *Journal of Petrology*, **42**, 2033–2048.

Frost, B.R., Lindsley, D.H. and Simmons, C. 1989. Penrose Conference Report – Origin and Evolution of Anorthosites and related rocks. *Geology*, **17**, 474–475.

Gawęda, A., Krzemińska, E. and Wiszniewska, J. 2009. A-type granites in the Mazury Complex – contribution to worldwide discussion on granite classification. *Przegląd Geologiczny*, **57**, 478–485. [In Polish]

Juskowiak, O. 1998. Occurrence, structure and mineral diversity of rocks from the Suwałki anorthosite massif. In: Ryka W. and Podemski M. (Eds), Geology of the Suwałki Anorthosite Massif (northeastern Poland). *Prace Państwowego Instytutu Geologiczego*, **61**, 53–80.

Kubicki, S. and Ryka, W. 1982. Geological Atlas of Crystalline Basement in Polish Part of East European Platform. Wydawnictwa Geologiczne; Warszawa. [In Polish]

Longhi, J., Vander Auwera, J., Fram, M. and Duchesne, J.C. 1999. Some phase equilibrium constraints on the origin of Proterozoic (Massif) anorthosites and related rocks. *Journal of Petrology*, **40**, 339–362.

Middlemost, E.A. 1994. Naming materials in the magma/igneous rock system. *Earth-Science Reviews*, **37**, 215–224.

Morgan, J.W., Stein, H.J., Hannah, J.L., Markey, R.J. and Wiszniewska, J. 2000. Re-Os study of Fe-Ti-V oxide and Fe-Cu-Ni sulfide deposits, Suwałki anorthosite massif, northeast Poland. *Mineralium Deposita*, **35**, 391–401.

Nekvasil, H. and Burnham, C.W. 1987. The calculated individual effects of pressure and water content on phase equilibria in the granite system. In: Mysen, B.O. (Ed.), Magmatic processes: Physicochemical Principles. *The Geochemical Society Special Publication*, **1**, 433–445.

Owens, B.E., Rockow, M.W. and Dymek, R.F. 1993. Jotunites from the Grenville Province, Quebec: petrological characteristics and implications for massif anorthosite petrogenesis. *Lithos*, **30**, 57–80.

Philpotts, A.R. 1981. A model for the generation of massif-type anorthosites. *The Canadian Mineralogist*, **19**, 233–253.

Ryka, W. 1993. Crystalline basement of Suwalszczyzna (NE Poland). *Przegląd Geologiczny*, **41**, 546–551. [In Polish]

Ryka, W. 1998. Geological position of the Suwałki Anorthosite Massif. In: Ryka, W. and Podemski, M. (Eds), Geology of the Suwałki Anorthosite Massif (northeastern Poland). *Prace Państwowego Instytutu Geologiczego*, **61**, 39–45.

Schärer, U., Wilmart, E. and Duchesne, J.C. 1996. The short duration and anorogenic character of anorthosite magmatism: U-Pb dating of the Rogaland complex, Norway. *Earth and Planetary Science Letters*, **139**, 335–350.

Shumlyanskyy, L., Hawkesworth, C., Billström, K., Bogdanova, S., Mytrokhyn, O., Romer, R., Dhuime, B., Cleasson, S., Ernst, R., Whitehouse, M. and Bilan, O. 2017. The origin of the Palaeoproterozoic AMCG complexes in the Ukrainian shield: New U-Pb ages and Hf isotopes in zircon. *Precambrian Research*, **292**, 216–239.

Stein, H.J., Morgan, J.W., Markey, R.J. and Wiszniewska, J. 1998. A Re-Os study of the Suwałki anorthosite massif, northeast Poland. *Geophysical Journal*, **4**, 11–114.

Streckeisen, A. 1974. How should charnockitic rocks be named? In: Bellière, J. and Duchesne, J.C. (Eds), Géologie Des Domaines Cristallins, pp. 349–360. Société Géologique de Belgique; Liège.

Taylor, S.R., Campbell, I.H., McCulloch, M.T. and McLennan, S.M. 1984. A lower crustal origin for massif-type anorthosites. *Nature*, **311** (5984), 372–374.

Thompson, R.N., Dickin, A.P., Gibson, I.L., Morrison, M.A. 1982. Elemental fingerprints of isotopic contamination of Hebridean Palaeocene mantle-derived magmas by Archaean sial. *Contributions to Mineralogy and Petrology*, **79**, 159–168.

Vander Auwera, J. and Longhi, J. 1994. Experimental study of a jotunite (hypersthene monzodiorite): constraints on the parent magma composition and crystallization conditions (P, T, fO_2) of the Bjerkreim-Sokndal layered intrusion. *Contributions to Mineralogy and Petrology*, **118**, 60–78.

Vander Auwera, J., Longhi, J. and Duchesne, J.C. 1998. A liquid line of descent of the jotunite (hypersthene monzodiorite) suite. *Journal of Petrology*, **39**, 439–468.

Wiszniewska, J., Claesson, S., Stein, H., Vander Auwera, J. and Duchesne, J.C. 2002. The north-eastern Polish anorthosite massifs: petrological, geochemical and isotopic evidence for a crustal derivation. *Terra Nova*, **14**, 451–460.

Wiszniewska, J. and Krzemińska, E. 2005. Precambrian Crystalline basement of northeastern Poland – new approach. *Mineralogical Society of Poland – Special Papers*, **26**, 97–104.

Wiszniewska, J. and Petecki, Z. 2014. A Mesoproterozoic titanomagnetite ore deposit in the Suwałki Anorthosite Massif and its geological environment. *Górnictwo Odkrywkowe*, **55**, 44–51. [In Polish]

Manuscript submitted: 15th February 2019
Revised version accepted: 8th May 2019